Korean Chem. Eng. Res., 60(1), 51-61 (2022)
https://doi.org/10.9713/kcer.2022.60.1.51
PISSN 0304-128X, EISSN 2233-9558

Mathematical Modelling and Simulation of CO_2 Removal from Natural Gas Using Hollow Fibre Membrane Modules

Boram Gu†

School of Chemical Engineering, Chonnam National University,
77 Yongbong-ro, Buk-gu, Gwangju, 61186, Korea
(Received 20 August 2021; Received in revised from 19 October 2021; Accepted 20 October 2021)

Abstract – Gas separation via hollow fibre membrane modules (HFMM) is deemed to be a promising technology for natural gas sweetening, particularly for lowering the level of carbon dioxide (CO_2) in natural gas, which can cause various problems during transportation and process operation. Separation performance via HFMM is affected by membrane properties, module specifications and operating conditions. In this study, a mathematical model for HFMM is developed, which can be used to assess the effects of the aforementioned variables on separation performance. Appropriate boundary conditions are imposed to resolve steady-state values of permeate variables and incorporated in the model equations via an iterative numerical procedure. The developed model is proven to be reliable via model validation against experimental data in the literature. Also, the model is capable of capturing axial variations of process variables as well as predicting key performance indicators. It can be extended to simulate a large-scale plant and identify an optimal process design and operating conditions for improved separation efficiency and reduced cost.

Key words: CO_2 separation, Natural gas, Hollow fibre membrane, Mathematical modelling

1. Introduction

Natural gas is considered to be one of the most crucial energy sources worldwide due to its environmental benefits compared to other fossil fuels [1,2]. It primarily consists of light hydrocarbons such as methane, ethane, propane and butanes with impurities of carbon dioxide, water and hydrogen sulphide, although their compositions may vary significantly depending on the production site [3]. In particular, acidic gases such as carbon dioxide (CO_2) can cause corrosion in the pipeline during transportation and therefore should be removed in order to control the gas quality for improved performance and to prevent any potential problems that can be caused during the process operation and transportation, e.g., the maximum CO_2 level is restricted to be < 3% [2]. CO_2 can be captured via absorption, adsorption and membranes; chemical absorption using amine solvents is a well-established technology for CO_2 capture. However, it requires high solvent regeneration energy and a large footprint [1,4,5]. Alternatively, membrane separation processes are thought to be promising; there are mainly two types of membrane separation methods applied for natural gas separation: gas separation via a selective membrane and chemical absorption via membrane contactor [2,6-13]. The latter is essentially similar to amine-based chemical absorption but operated in a membrane contactor. Such a gas-liquid membrane contactor system carries similar disadvantages accompanied by the use of amine solvents. On the other hand, membrane gas separation is induced by a partial pressure difference between feed and permeate gases. It has several advantages such as simple equipment, small footprint, easy operation and maintenance and cost-effectiveness and therefore is considered to be an efficient alternative to the conventional absorption method [7,14]. However, membrane gas separation has several limitations, such as low CO_2 fluxes and selectivities and high operating cost for gas compression [9].

Many attempts have been made to improve the separation performance, especially around developing new polymeric membranes [6,14-23]. In particular, the membrane needs to possess a good gas permeability and selectivity, but they are often in a trade-off relationship [6]. In addition to membrane materials, the membrane module design plays a critical role in determining separation efficiency [3,24-26]. There are three types of membrane modules – plate-and-frame, spiral-wound and hollow fibre modules – among them, a hollow fibre membrane module (HFMM) is a popular option owing to its high packing density [24]. Not only are the diameter and thickness of membrane fibres critical, but the diameter and length of the membrane module containing the bundle of hollow fibres are also important. Furthermore, for a large-scale separation plant, process design and operating conditions should be carefully selected via optimisation for improved performance and reduced cost [5,27].

Mathematical modelling can be a valuable and efficient tool in deriving an effective process design and operation strategy. Depending on the selected membrane materials and module, separation performance can be predicted for a single module, as well as other process variables such as flowrate, concentration and pressure.

† To whom correspondence should be addressed.
E-mail: boram.gu@jnu.ac.kr

Furthermore, by extending the model, simulation for a large-scale plant with multiple HFMMs can be undertaken in order to assess plant performance, energy consumption and cost. There are a number of modelling and simulation studies for HFMM in the literature [3,4,18,25-37]. Lock et al. developed a model for CO_2 capture using HFMM by means of Aspen HYSYS in order to facilitate the integration of HFMM in the entire natural gas purification plant [34]. Although their model incorporates a radial crossflow within HFMM to take into account more realistic flow effects on separation performance and cost, their work focused on analysing predicted spatial pressures and overall performance and cost without detailed analyses on spatial variations in flowrates and compositions. Moreover, Chu et al. presented a mathematical modelling approach using orthogonal collocation to approximate nonlinear differential equations [3]. Although the models presented in the literature proved their competency in calculating the overall performance indicators, the treatment of boundary conditions for model equations, especially at the closed end of the permeate side, was not addressed or assumed to be zero, which is not realistic. In general, one side of permeate side is closed, meaning that there is only an exit of the permeate flow path. In a steady-state, permeate flowrate and composition at the closed end are not zero and depend on permeate fluxes across the membrane. Therefore adequate boundary conditions for the permeate side should be applied so as to identify the steady-state permeate flowrate and composition at the permeate closed end. Furthermore, an iterative numerical procedure is required to apply such implicit boundary conditions and solve a set of nonlinear differential equations to resolve flowrate, concentration and pressure profiles.

This study aims to develop a tractable mathematical model for hollow fibre gas separation with an efficient numerical procedure to obtain model solutions. In particular, the treatment of boundary conditions for the differential model equations is focused to realistically resolve permeate fluxes, flowrates and compositions, especially at the closed permeate end. The developed model is validated against experimental data available in the literature [37,38] to ensure the reliability of the model. Simulations under various operating conditions and flow modes for removing carbon dioxide from natural gas (assumed to be methane, CH_4) are undertaken to investigate the effects of those variables on the overall separation performance.

2. Methods

2-1. Overview of a modelling approach

Fig. 1 shows a schematic illustration of HFMM with various operation modes. Key module design parameters involve a module diameter (d_{md}), effective fibre length (L), the number of fibres (N) and inner and outer diameters of a single fibre (d_i and d_o), shown in Fig. 1a. Feed gas can enter either the bundled hollow fibres or the membrane module side (i.e., outside the bundled hollow fibres), making the permeate gas flow outside or inside the fibres. The former is called the feed-tube (FT) mode, and the latter the feed-shell (FS) mode, as depicted in Fig. 1b. Also, two gas streams, feed and permeate, can be

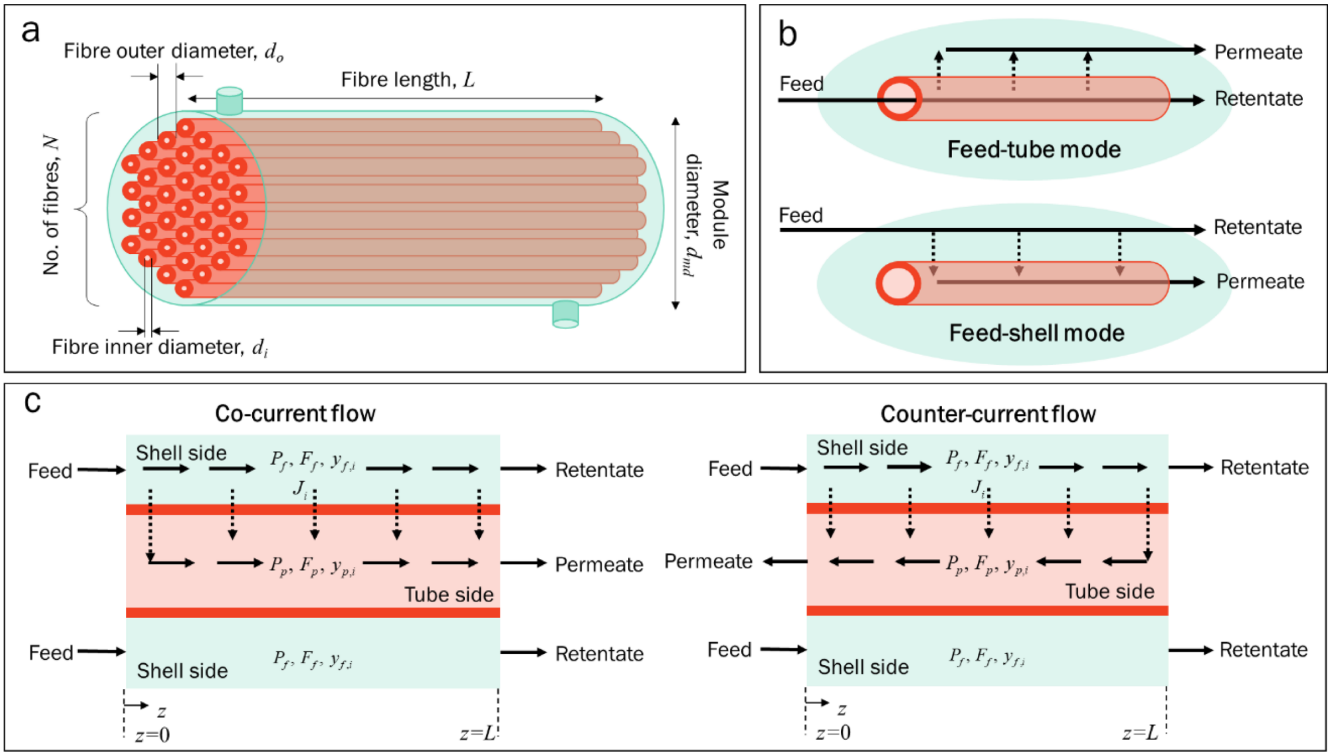

Fig. 1. A schematic of hollow fibre membrane module (HFMM) and flow configurations. a: an illustration of HFMM and key module design parameters, b: two flow modes, feed gas flowing inside fibres (feed-tube mode, FT) and feed gas flowing outside fibres (feed-shell mode, FS), c: two flow directions, co-current (CO) and counter-current (CT) flow.

either in the co-current (CO) or counter-current (CT) flows. As a result, there are four flow configurations: co-current & feed-tube (CO-FT), counter-current & feed-tube (CT-FT), co-current & feed-shell (CO-FS) and counter-current & feed-shell (CT-FS) modes. In addition, sweep gas, either inert gas or retentate, can be imposed on the permeate side to induce a higher driving force for permeation through the membranes. This study only takes into account operating scenarios without sweep gas, as illustrated in Fig. 1a.

2-2. Mathematical modelling

There are several assumptions used to develop a mathematical model for HFMM at the steady-state. First of all, an axial gas stream direction in the shell side is assumed due to the trivial portion of non-axial flow near the entrance and exit of the module. In other words, there are either perfect co-current or counter-current flows. Second, radial variations in flow and concentration patterns are neglected both in the tube and shell, i.e., plug flow. Third, all fibres are assumed to be aligned axially and distributed uniformly, making the cross-sectional areas of tube and shell sides constant across the membrane module. Finally, temperature variations in the membrane materials and inside the module are assumed to be negligible due to isothermal operation.

The amount of gas passing through the membrane is governed by the difference of partial pressures between the feed and permeate sides, formulated by the following equation.:

$$J_i = Q_i \left(P_{f,i} - P_{p,i} \right) \tag{1}$$

where J_i is the permeate flux of component i in mol/(m^2·s), Q_i the membrane permeance for component i in mol/(Pa·m^2·s), P_i the partial pressure of component i in Pa. The subscripts f and p denote feed and permeate, respectively. Partial pressure is determined by the total pressure and molar fraction of each component as:

$$P_{k,i} = y_{k,i} P_k \quad \text{for } k = f \text{ or } p \tag{2}$$

where P_k and $y_{k,i}$ is the total pressure and molar fraction of component i either for feed or permeate streams, respectively.

The component balances for each feed and permeate side are formulated as follows:

$$\frac{dF_{f,i}}{dz} = -J_i W_{int} \tag{3}$$

$$\frac{dF_{p,i}}{dz} = \begin{cases} J_i W_{int} & \text{for co-current} \\ -J_i W_{int} & \text{for counter-current} \end{cases} \tag{4}$$

$$W_{int} = \pi d_o N \tag{5}$$

where F_i is the molar flowrate of component i in mol/s and W_{int} the interfacial membrane width in m. By solving Eqs. (3) and (4), axial molar flowrates can be obtained, along with molar fractions of each component using Eq. (6).

$$y_{k,i} = \frac{F_{k,i}}{\sum_i F_{k,i}} \quad \text{for } k = f \text{ or } p \tag{6}$$

Axial pressure variations are accounted for via pressure drop equations derived from the Hagen-Poiseuille equation for ideal gases. The pressure drop equations can be found in the literature [3], depending on the flow configurations.

A set of ordinary differential equations in Eqs. (3)-(4) and pressure drop equations is solved using the following boundary conditions. For the feed stream, inlet conditions (at $z = 0$) are given:

$$F_{f,i} = y_{f,i}^{in} F_f^{in} \quad \text{at } z = 0 \tag{7}$$

$$P_f = P_f^{in} \text{ at } z = 0 \tag{8}$$

where F_f^{in}, y_f^{in} and P_f^{in} are the inlet feed flowrate, molar fraction and pressure, respectively. Boundary conditions for permeate flowrates and pressures are given differently for the co-current and counter-current flow. For the co-current flow, the derivative of each permeate flowrate at the closed end (at $z = 0$) is provided as a boundary condition, which equals the product of permeate flux and interfacial width for each component, as shown in Eq. (9).

$$\frac{dF_{p,i}}{dz} = J_i W_{int} \quad \text{at } z = 0 \quad \text{for co-current flow} \tag{9}$$

On the other hand, permeate flowrate at the exit (at $z = 0$) is the integration of permeate flux along the axial direction, as in Eq. (10).

$$F_{p,i} = \int_{z=0}^{z=L} J_i W_{int} dz \quad \text{at } z = 0 \quad \text{for counter-current flow} \tag{10}$$

Permeate pressure at the exit is assumed to be atmospheric, which are given in Eqs. (11) and (12) for the co-current and counter-current modes, respectively.

$$P_p = 1 \text{atm at } z = L \quad \text{for co-current flow} \tag{11}$$

$$P_p = 1 \text{atm at } z = 0 \quad \text{for counter-current flow} \tag{12}$$

2-3. Numerical algorithm and simulation details

The ordinary differential equations in Eqs. (3)-(4) and pressure drop equations are converted to a set of algebraic equations through the 1st order finite backward difference method. The derivative and integral terms in the boundary conditions in Eqs. (9)-(10) are reformulated to algebraic equations and applied to solve the above model equations. For the permeate side, an iterative procedure is required to apply the boundary conditions and solve the differential equations simultaneously by obtaining values of $F_{p,i}$ and P_p at $z = 0$ for the co-current mode and $F_{p,i}$ at $z = 0$ for the counter-current mode, as illustrated in Fig. 2. The modified fixed-point iteration method is applied to update unknown variables, for example,

$$\mathbf{x}^{new} = \mathbf{x}^{old} + \kappa \mathbf{e} \tag{13}$$

where $\mathbf{x}$ is the variable to be found, $\mathbf{e}$ the relative errors defined

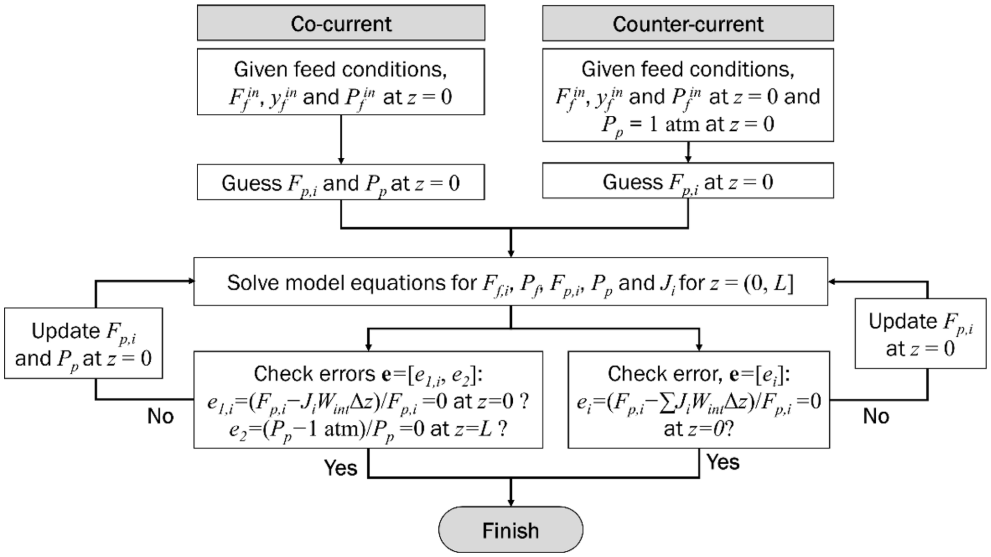

Fig. 2. A numerical algorithm used in this study.

in Fig. 2 and κ the constant between 0 and 1 that controls the convergence speed and numerical stability. For example, for a binary system of CO_2 and CH_4, three variables, $F_{p,CO2}$, $F_{p,CH4}$ and P_p at $z = 0$ should be found for the co-current flow, while two variables, $F_{p,CO2}$ and $F_{p,CH4}$ are obtained for the counter-current flow.

A number of simulations are undertaken by varying feed flowrate, composition and pressure for four different flow configurations, i.e., CO-FS, CO-FT, CT-FS and CT-FT. It is assumed that feed gas is composed of methane (CH_4) and CO_2. For different operating conditions, key performance variables – a stage cut defined by a ratio of the total permeate to inlet feed flowrate, CH_4 composition in the retentate and CO_2 composition in the permeate – are analysed and compared. The specifications of HFFM and operating conditions used in the simulation are listed in Table 1. The range of varying conditions is chosen based on the literature [3]. A wide range of feed flowrate is chosen to span between 0 and 100% of the resultant stage cut. For model discretisation, the number of segments (N_z) is selected to be sufficiently large so that the aforementioned key performance indicators are independent of a chosen segment size; for a 0.6 m fibre, discrepancies in the calculated stage cut are less than 1% among N_z of 100, 200 and 400 without a noticeable difference in computation time. The model equations and numerical algorithm are implemented in an in-house code programmed in MATLAB.

3. Results and Discussion

First, the developed model is validated against experimental data available in the literature [31,38], followed by simulation results under various operating conditions.

3-1. Model validation

Fig. 3 shows comparison results between experimental data and simulation results of CH_4 composition in the retentate stream for four flow configurations under the same experimental conditions [37]; feed gas consists of CH_4 and CO_2 at $T = 301$ K, $P_f^{in} = 405.3$ kPa, $y_{f,CO2}^{in} = 0.6$. Membrane permeances for each component are: $Q_{CO2} = 1.48\times10^{-9}$ mol/(m^2·Pa·s) and $Q_{CH4} = 4.12\times10^{-10}$ mol/(m^2·Pa·s). In the experiments, a composite membrane of a polysulfone support layer and aliphatic copolymer coating was used. Module specifications

Table 1. Simulation conditions used in this work

Description	Symbol	Value	Unit	Source
Temperature	T	296.15	K	-
Feed pressure	P_f^{in}	20×10^5, 40×10^5 and 60×10^5	Pa	-
Feed flowrate	F_f^{in}	8.4×10^{-3} to 6.65	mol/s	-
Feed CO_2 composition	$y_{f,CO2}^{in}$	0.05, 0.1, 0.2 and 0.3	-	-
CO_2 permeance	Q_{CO2}	3.207×10^{-9}	mol/(m^2·Pa·s)	[3]
CH_4 permeance	Q_{CH4}	1.33×10^{-10}	mol/(m^2·Pa·s)	[3]
Module diameter	d_{md}	0.1	m	[3]
Fibre outer diameter	d_o	250×10^{-6}	m	[3]
Fibre inner diameter	d_i	200×10^{-6}	m	[3]
Fibre length	L	0.6	m	[3]
Number of fibres	N	60,000	-	[3]
Number of discretised segments	N_z	400	-	-

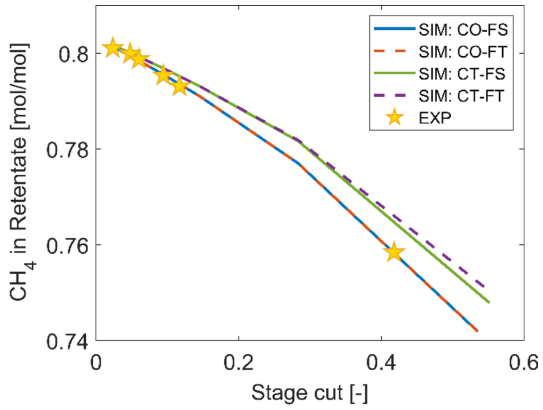

Fig. 3. Comparison between the calculated mole fraction of CH_4 from the developed model and experimental data for the CH_4-CO_2 system [37]. Solid and dashed lines are simulation results, and star symbols are experimental data.

are: d_{md} = 0.01 m, $d_o = 735\times10^{-6}$ m, $d_i = 389\times10^{-6}$ m, L = 0.15 m and N = 100. Comparison results demonstrate that the calculated CH_4 mole fraction in the retentate stream for the co-current flow is in good agreement with the reported experimental data in the literature [37] at a relative error of up to 0.054% in the retentate CH_4 composition, although the experimental flow mode was not clearly stated.

In addition, a binary system of N_2 and O_2 is simulated and compared with an experimental study in the literature where asymmetric hollow fibre membranes with a dense outer layer and porous support were used [38]. The experiments were undertaken for all four flow configurations: CO-FS, CO-FT, CT-FS and CT-FT. The experimental conditions are: T = 296.15 K, P_f^{in} = 790.8 kPa, $y_{f,O2}^{in}$ = 0.205, $Q_{O2} = 3.078\times10^{-9}$ mol/(m^2·Pa·s) and $Q_{N2} = 5.7\times10^{-10}$ mol/(m^2·Pa·s), $d_{md} = 9.5\times10^{-3}$ m, $d_o = 160\times10^{-6}$ m, $d_i = 80\times10^{-6}$ m, L = 0.25 m and N = 368. As can be seen in Fig. 4, calculated N_2 composition in the retentate and O_2 composition in the permeate by the developed model show a good agreement with the experimental results; relative errors between the model and experiments in the N_2 and O_2 compositions are less than 0.6% and 1.4%, respectively. The model validation results presented here demonstrate the credibility of the developed model for a CO_2-CH_4 system and an air separation system. Based on the comparison results, it is also believed that the model can be extended for multicomponent systems and would be able to produce reliable predictions if permeance parameters are accurately measured via experiments, as in the aforementioned experimental studies.

3-2. Simulation results of a representative case

Spatial variations in flowrates, permeate fluxes, mole fractions and pressures in the feed and permeate sides are presented in Figures 5 and 6 for CO and CT modes, respectively. Both simulations are in FS mode at $P_f^{in} = 60\times10^5$ Pa, F_f^{in} = 0.175 mol/s and $y_{f,CO2}^{in}$ = 0.1 with other operating conditions as listed in Table 1. Simulation results reveal that CT achieves a larger stage cut, CH_4 purity of the retentate and CO_2 composition of the permeate than CO, although differences are small, i.e., stage cut: 21.45% and 21.82%, CH_4 purity of 98.80% and 99.38% and CO_2 purity of 42.55% and 43.63% for CO and CT, respectively. Furthermore, the separation factor, defined by $(y_{p,CO2}/y_{p,CH4})/(y_{f,CO2}/y_{f,CH4})$, is predicted to be 61.3 and 125 for CO and CT, respectively. The high separation factor for CT is attributed to the CO_2 mole fraction in the retentate being almost 0.

In CO shown in Fig. 5, CO_2 flux decreases along the flow direction (from 1.68×10^{-3} to 9.15×10^{-5} mol/(m^2·s)) while CH_4 flux remains relatively constant over the membrane module (from 7.14×10^{-4} to 7.81×10^{-4} mol/(m^2·s)). This is mainly attributed to the high CO_2 permeance, which leads to rapid CO_2 permeation under the high driving force near the module entrance. Because of the loss of CO_2 in the feed stream, the CO_2 feed flowrate ($F_{f,CO2}$) decreases as well as its mole fraction in the feed stream ($y_{f,CO2}$), as shown in Figs. 5b and 5c. Likewise, the CH_4 flowrate in the feed side is reduced along the flow direction due to the continuous permeation of CH_4 through the

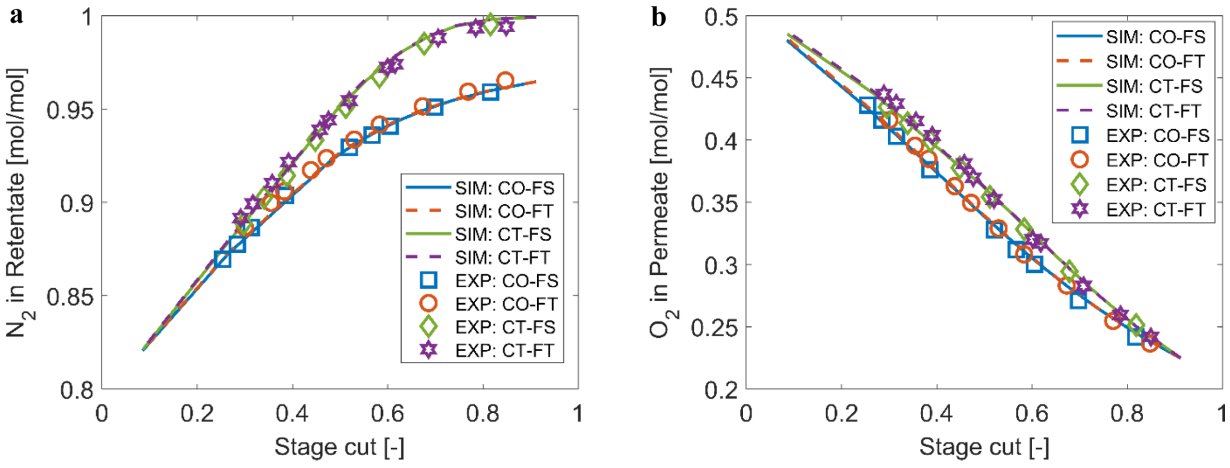

Fig. 4. Comparison between simulation results and experimental data for the N_2-O_2 system [38], a: N_2 mole fraction in the retentate stream and b: O_2 mole fraction in the permeate stream. Solid and dashed lines are simulation results, and square, circle, diamond and hexagram symbols are experimental data.

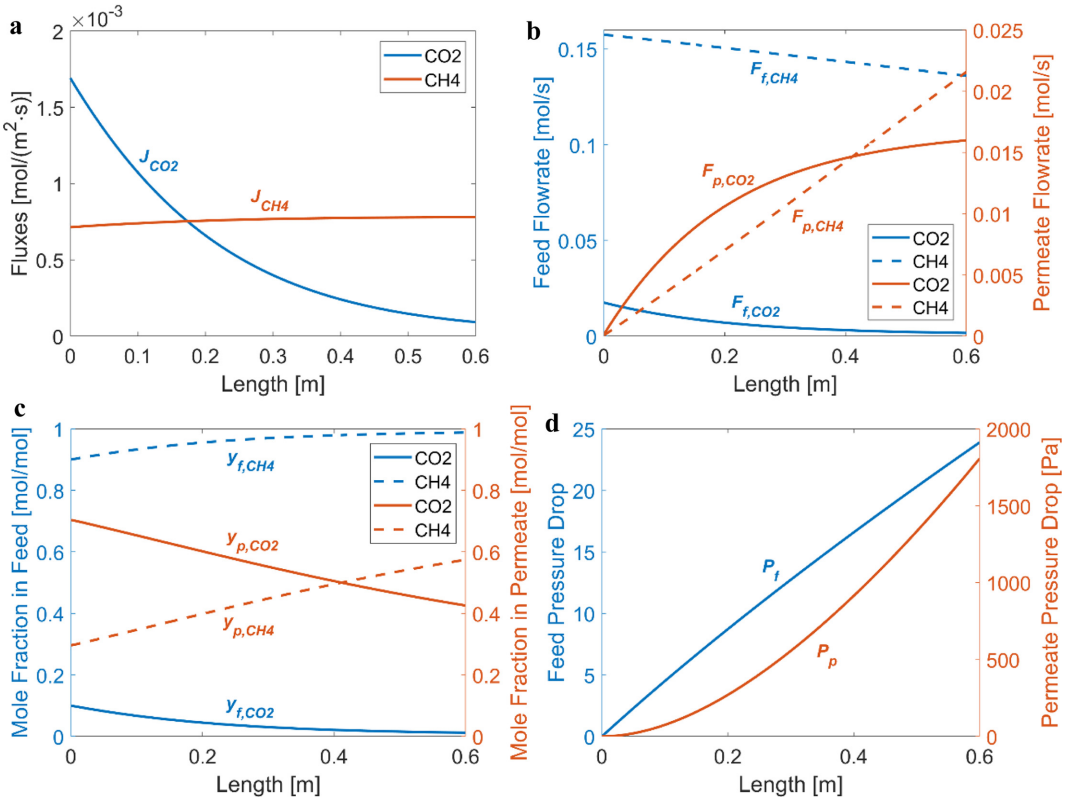

Fig. 5. Spatial variations of flowrates, fluxes mole fractions and pressures in the feed and permeate sides for the co-current flow. a: CO_2 and CH_4 fluxes, b: (left axis) CO_2 and CH_4 flowrates in the feed side, (right axis) CO_2 and CH_4 flowrates in the permeate side, c: (left axis) CO_2 and CH_4 mole fraction in the feed side, (right axis) CO_2 and CH_4 mole fraction in the permeate side, d: (left axis) feed pressure drop defined as ($P_{f,in} - P_f$), (right axis) permeate pressure drop defined as ($P_p - P_{p,out}$ (1atm)). In b-d, blue and orange curves correspond to the left and right axes, respectively.

membrane, but its mole fraction CH_4 increases. This results from the larger amount of CO_2 permeation through the membrane than CH_4. As can be seen in Fig. 5d, pressure drops in both feed and permeate sides are insignificant, which means the mole fraction of each component is a critical factor in determining permeate fluxes. As demonstrated in Fig. 5c, the difference of CO_2 mole fraction between the feed and permeate side decreases, which coincides with decreasing CO_2 flux along the flow direction, as shown in Fig. 5a.

CT achieves CO_2 flux of 1.78×10^{-3} to 8.82×10^{-5} mol/(m^2·s) and CH_4 flux of 7.11×10^{-4} to 7.81×10^{-4} mol/(m^2·s), with remarkable similarity of the axial profile to CO, as shown in Fig. 6a and Fig. 5a for CT and CO, respectively. However, the patterns of flowrates, mole fractions and pressures in CT appear to be different from those in CO owing to the opposite direction of permeate flow. As seen in Fig. 6b, the permeate flowrate increases in the permeate flow direction, i.e., from $L = 0.6$ m to $L = 0$ m, which appears to be flipped horizontally from the permeate flowrate patterns in CO shown in Fig. 5b.

Interestingly, the trend of mole fractions in CT resembles that in CO despite the opposite direction of permeate streams in CO and CT, i.e., a decrease of CO_2 mole and an increase of CH_4 in the permeate side from $L = 0$ m to 0.6 m. In other words, the CO_2 mole fraction rises towards the permeate exit (from approximately 0.1 to 0.4), unlike decreasing the CO_2 mole fraction in CO (from around 0.7 to 0.4). Also, the CH_4 mole fraction decreases from about 0.9 to 0.6 towards the permeate exit, while CO exhibits an increase in the CH_4 mole fraction from around 0.3 to 0.6 toward the exit. This could be due to the dominant role of feed pressure and mole fractions in calculating fluxes, which make the permeate mole fractions follow the trends of feed mole fractions. Nevertheless, both CO and CT configurations result in the almost same exit mole fractions in the permeate side.

It is noticed that permeate pressures at the closed end in both flow configurations differ from each other, i.e., differences between the closed end pressure and exit pressure (1 atm) are 1190 Pa and 1806 Pa for CT (Fig. 6(d)) and CO (Fig. 5(d)), respectively. This implies that CT might be more advantageous than CO in terms of relatively small pressure loss along the permeate side. The same is observed for FT scenarios (omitted here due to similar trends to FS); 243.4 Pa vs 145.4 Pa for CO and CT flows, respectively. Nevertheless, it should be noted that pressure drops could become significant depending on the module and fibre specifications, more precisely the fibre inner diameter and packing density determined by the number of fibres, module diameters and outer fibre diameter.

Fig. 7 displays the simulation results of CO_2 mole fraction in the permeate and CH_4 in the retentate for four flow configurations under the same operating conditions as those used for Figs. 5 and 6. Feed

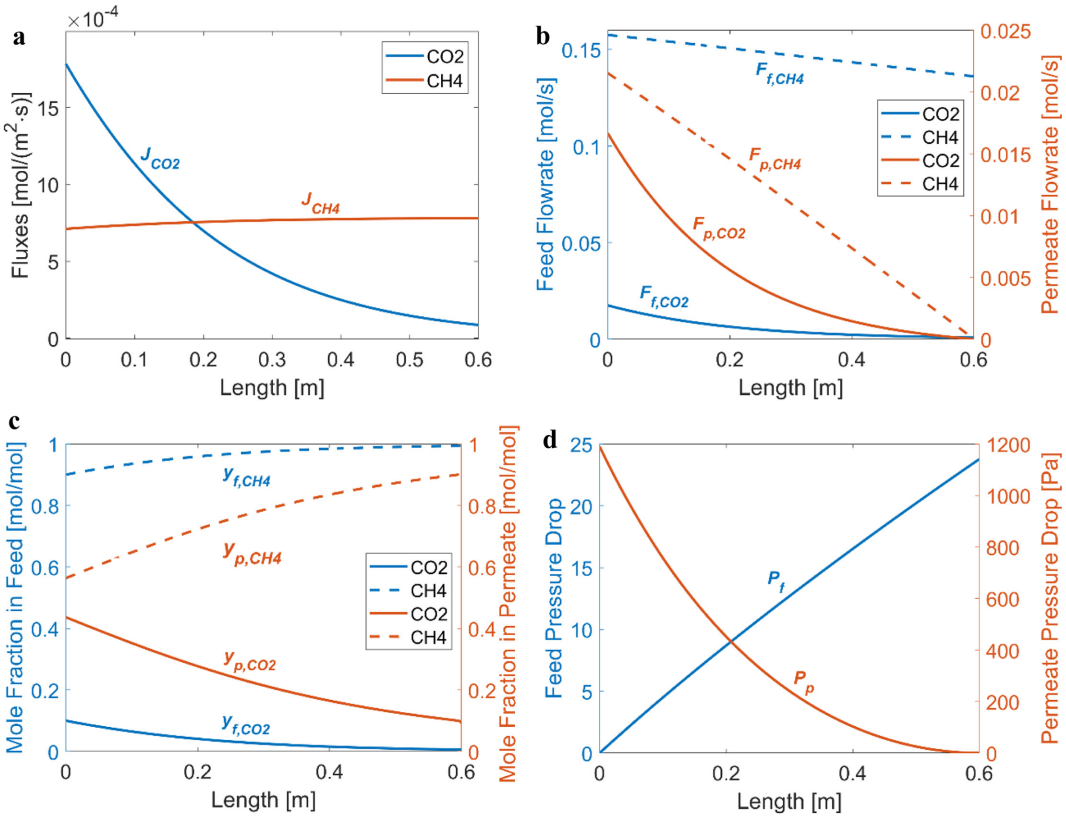

Fig. 6. Spatial variations of flowrates, fluxes, mole fractions and pressures in the feed and permeate sides for the counter-current flow. a: CO_2 and CH_4 fluxes, b: (left axis) CO_2 and CH_4 flowrates in the feed side, (right axis) CO_2 and CH_4 flowrates in the permeate side, c: (left axis) CO_2 and CH_4 mole fraction in the feed side, (right axis) CO_2 and CH_4 mole fraction in the permeate side, d: (left axis) feed pressure drop defined as ($P_{f,in} - P_f$), (right axis) permeate pressure drop defined as ($P_p - P_{p,out}$ (1atm)). In b-d, blue and orange curves correspond to the left and right axes, respectively.

flowrate is varied between 0.03 mol/s and 1.7 mol/s to accomplish a stage cut of 3.6% to 86%. It is worth mentioning that a stage cut is one of the main performance indicators in gas separation via membranes, which is determined by a feed flowrate and module length. As the feed flowrate increases at the fixed module length, a resulting stage cut decreases because the total permeate flowrate relative to the feed is reduced, as demonstrated in Fig. 7. An important finding is that for a high stage cut, high CH_4 purity in the retentate, up to almost 100%, can be achieved, whereas CO_2 composition in the permeate is lowered. This suggests that if gas separation aims to improve natural gas quality, a high stage cut operation should be favourable at the expense of CO_2 purity.

It can also be seen that there is a negligible difference between FS and FT modes for the current membrane specifications. Furthermore, as mentioned earlier, differences between CO and CT are not pronounced, although only CT is able to reach close to 100% separation. It can be observed that the CO_2 mole fraction in the permeate tends to its initial mole fraction of the feed gas as increasing stage cut due to higher CO_2 permeance than CH_4 permeance.

Prior to further simulations under various conditions, the current numerical method that accounts for the steady-state boundary conditions at the closed end of the permeate side is compared with a simulation that assumes zero permeate flowrates at the closed end (called the

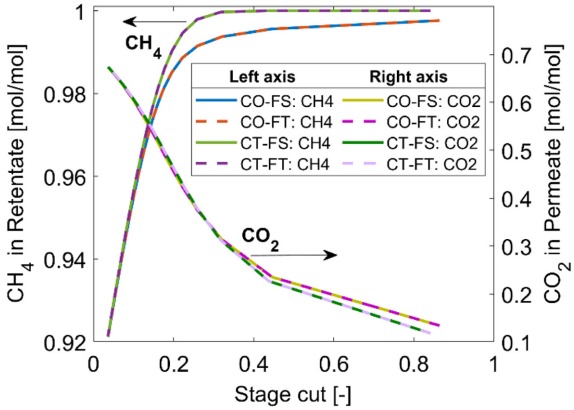

Fig. 7. Simulation results at $P_f = 60\times10^5$ Pa and $y_{f,CO2} = 0.1$ for four flow configurations by varying a feed flowrate between 0.030 mol/s and 1.7 mol/s. (Left axis) CO_2 mole fraction in the permeate and (right axis) CH_4 mole fraction in the retentate.

simplified method). The simulation conditions are same as those used in the representative scenario. Overall performance indicators resulting from two simulations exhibit small differences; a stage cut of 21.46% for the current method and 21.37% for the simplified method. However, there is a noticeable difference in spatial profiles, especially near the closed end of the permeate side. As can be in Fig. 8b, imposing zero permeate flowrates for each component at the closed

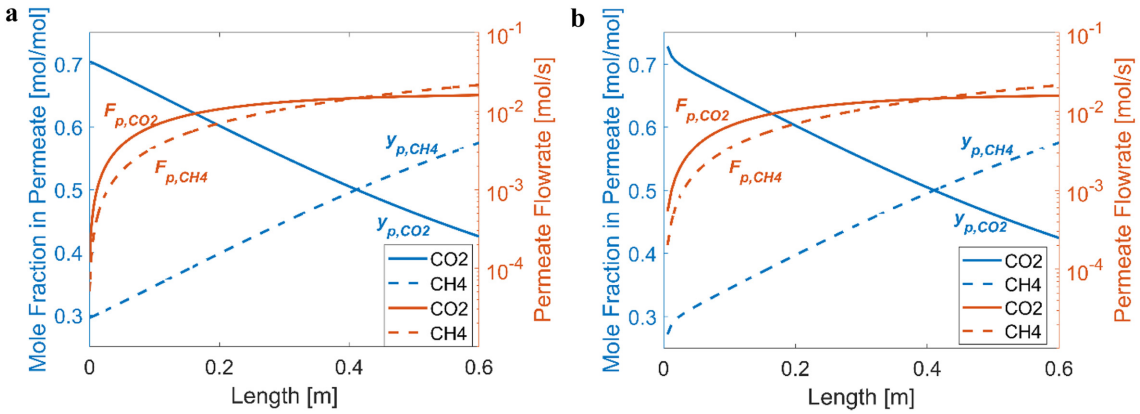

Fig. 8. Permeate flowrates and molar compositions predicted by the current method (with the steady-state permeate flowrates at the closed end) and simplified method (with zero permeate flowrates at the closed end). a: using the current numerical method, b: the simplified method. A logarithmic scale is used for the right y-axis, permeate flowrate.

end results in the loss of information at the closed end of the permeate side. This leads to the distinct curve of molar fractions near $z = 0$. On the other hand, using the steady-state permeate flowrates obtained by the proposed numerical method, smooth curves can be gained for molar fractions, as demonstrated in Fig. 8a.

3-3. Simulation results under various operating conditions

In this section, simulation results under different feed pressures and compositions for CO and CT are presented for the FS mode. First of all, the dependence of stage cut on feed flowrate under different feed conditions is shown in Fig. 9. There is no noticeable difference between CO and CT for all conditions, consistent with the representative case presented earlier. It is demonstrated that there is a lower limit of feed flowrate for a fixed module design, which makes the resulting stage cut close to 100%. Also, the stage cut becomes dramatically reduced as the feed flow increases, which implies that the practical range of feed flowrate would be narrower than the whole simulated range (from 0.0084 mol/s up to 5.25 mol/s) that corresponds to a stage cut of 1% to 100% for a single HFFM. If multiple HFFMs are to be used in the natural gas purification process, an operating feed flowrate can be decided depending on the target single stage cut via model calculation.

The effects of feed composition on the predicted stage cuts can be analysed; for the fixed feed flowrate, a stage cut is larger as the CO_2 composition in the feed becomes larger. This can be explained by CO_2 fluxes being larger than CH_4 fluxes for the simulated membrane module. Feed pressure also demonstrated its influence on the predicted stage cut, as can be seen in Fig. 8. The larger the feed pressure, the larger the stage cut achieved at the constant feed flowrate. This is a reasonable outcome because the main driving force for permeation is a partial pressure difference between the feed and permeate sides.

An interesting observation can be made that patterns of separation factors ($=(y_{p,CO2}/y_{p,CH4})/(y_{f,CO2}/y_{f,CH4})$) in CT differ significantly from those in CO, especially at low feed flowrates, i.e., at high stage cuts. In such conditions, CH_4 purity in the retentate tends to 1, which makes the separation factor approach infinity, as can be seen in Fig. 8b. On the other hand, there seems to be an optimal feed flowrate that can achieve the maximum separation faction when the system is in CO. Further results of CH_4 and CO_2 compositions in the retentate and permeate streams will be addressed below.

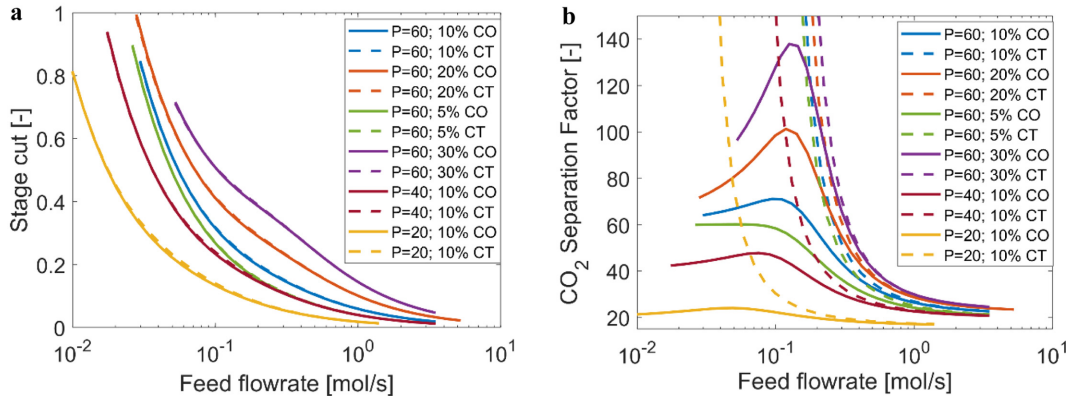

Fig. 9. Simulation results with respect to varied feed flowrate. a: Predicted stage cut vs feed flowrate in the logarithmic scale and b: separation factor $(y_{p,CO2}/y_{p,CH4})/(y_{f,CO2}/y_{f,CH4})$ under various operating conditions for the FS mode. P indicates feed pressures (20×10^5 Pa, 40×10^5 Pa and 60×10^5 Pa), and the percentage values denote feed CO_2 molar compositions (5%, 10%, 20% and 30%).

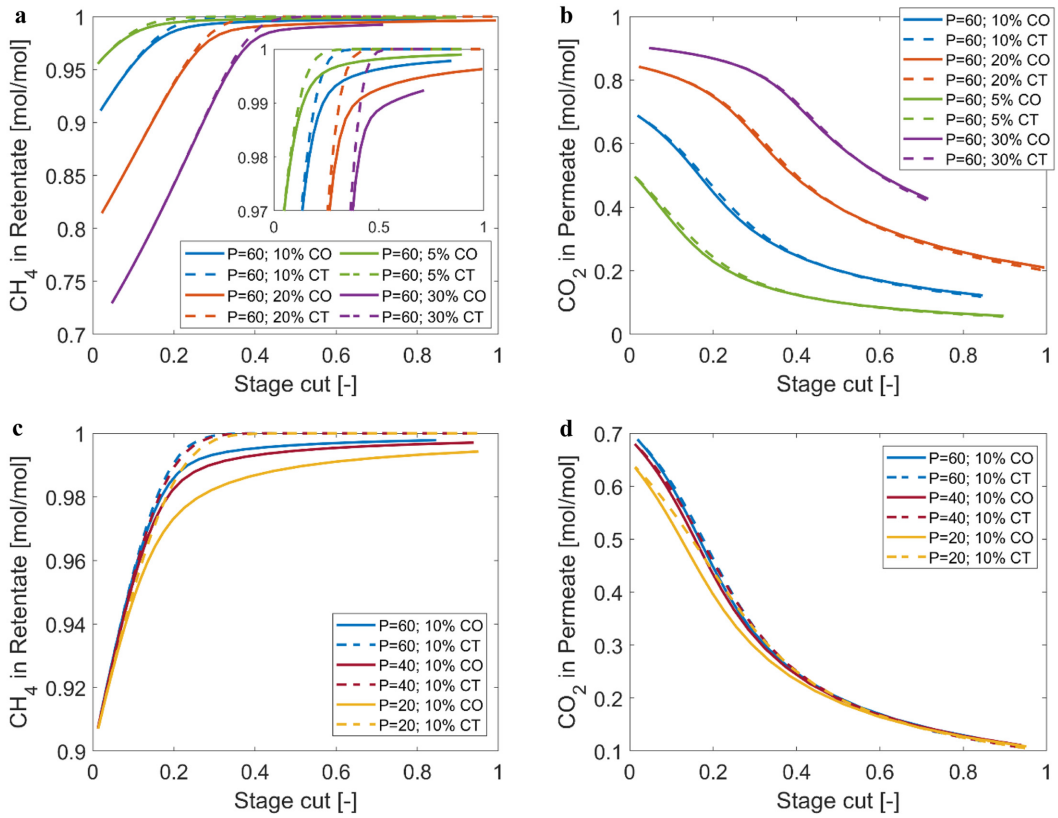

Fig. 10. Simulation results under various operating conditions for the feed-shell mode. P indicates feed pressures (20×10^5 Pa, 40×10^5 Pa and 60×10^5 Pa), and the percentage values denote feed CO_2 molar compositions (5%, 10%, 20% and 30%). a: predicted CH_4 composition in the retentate vs predicted stage cut under varying feed composition, b: predicted CO_2 composition in the permeate vs predicted stage cut under varying feed composition, c: predicted CH_4 composition in the retentate vs predicted stage cut under varying feed pressure and d: predicted CO_2 composition in the permeate vs predicted stage cut under varying feed pressure.

Fig. 10 displays the CH_4 mole fraction in the retentate and CO_2 mole fraction in the permeate under various operating conditions with respect to the predicted stage cut for varied feed flowrates. The top figures (Figures 10 a-b) can be used to investigate the effects of feed compositions on the resultant CH_4 purity in the retentate and CO_2 composition in the permeate. Although the CH_4 composition varies in a range of 70% to 95%, all the simulated scenarios can achieve a purity over 99% at a feed pressure of 60 bar. As a stage cut increases (i.e., feed flowrate decreases), purification performance is shown to be improved. An interesting observation in Fig. 10a (the zoomed plot) is that discrepancy between CO and CT modes is larger at the lower CH_4 composition in the feed stream. This implies that CT should be preferred in such cases where the amount of impurities in natural gas is significant.

For the CO_2 mole fraction in the permeate stream in Fig. 10b, the same trends are observed in Fig. 7 for the representative case. Obviously, the composition of CO_2 in the permeate is higher for higher CO_2 feed compositions. Due to the inherent nature of the selected membrane with its CO_2 and CH_4 permeance values, there is a maximum CO_2 mole fraction that can be achieved even at the very small stage cut. Also, as mentioned earlier in the previous section, the CO_2 mole fraction tends to the feed CO_2 mole fraction as the stage cut approaches 1.

Furthermore, the retentate and permeate compositions are affected by feed pressures as displayed in Figs. 10c and 10d, albeit not significantly. Higher feed pressures lead to higher CH_4 composition in the retentate and higher CO_2 composition in the permeate. Interestingly, differences between CO and CT in CH_4 in the retentate shown in Figure 10c are more pronounced at lower feed pressures. All CT scenarios achieve 100% CH_4 in the retentate, while for CO, the CH_4 mole fraction at 100% stage cut is slightly lower than 1. Therefore it can be said from Fig. 10c that CT outperforms CO in terms of CH_4 purity while there might be an insignificant difference between CT and CO in a scenario where a stage cut is expected to be very low.

4. Conclusion

In this study, we develop a tractable mathematical model for gas separation via hollow fibre membrane modules which can be applied to various gas mixture systems. The model is capable of not only predicting a production rate and purity but also capturing spatial profiles of flowrates, compositions and pressures both in the feed and permeate sides through imposing appropriate steady-state boundary

conditions for the differential model equations. Furthermore, four types of flow mode (CO-FS, CO-FT, CT-FS and CT-FO) are accounted for in the model, which makes the developed model applicable to optimisation an operation mode for performance improvement.

Model validation results demonstrate an excellent agreement with two sets of experimental data in the literature; the first set of data was for a CO_2-CH_4 system with an arbitrary flow mode, and the other was for an O_2-N_2 system with all four flow modes. The developed model has proven its potential for a wide range of gas separation applications, in addition to natural gas sweetening. The current model can be extended to simulate a large scale separation process with multiple membrane modules to assess the large scale performance. Furthermore, model-based optimisation can be performed to identify an optimal process design and operating conditions to achieve improved performance and reduced cost by coupling a cost model with the developed model.

Acknowledgement

This work is supported by the National Research Foundation of Korea (NRF) grant funded by the Korea government (MSIT) (No. 2021R1C1C1006287).

References

1. Chu, Y. and He, X., "Process Simulation and Cost Evaluation of Carbon Membranes for CO_2 Removal from High-Pressure Natural Gas," *Membr.*, **8**(4), 118(2018).
2. Rufford, T. E., Smart, S., Watson, G. C. Y., Graham, B. F., Boxall, J., Diniz da Costa, J. C. and May, E. F., "The Removal of CO_2 and N_2 from Natural Gas: A Review of Conventional and Emerging Process Technologies," *J. Pet. Sci. Eng.*, **94-95**, 123-154(2012).
3. Chu, Y., Lindbråthen, A., Lei, L., He, X., and Hillestad, M., "Mathematical Modeling and Process Parametric Study of CO_2 Removal from Natural Gas by Hollow Fiber Membranes," *Chem. Eng. Res. Des.*, **148**, 45-55(2019).
4. Hosseini, S. S., Dehkordi, J. A. and Kundu, P. K., "Mathematical Modeling and Investigation on the Temperature and Pressure Dependency of Permeation and Membrane Separation Performance for Natural Gas Treatment," *Chem. Prod. Process Model.*, **11**(1), 7-10(2016).
5. He, X., "A Review of Material Development in the Field of Carbon Capture and the Application of Membrane-Based Processes in Power Plants and Energy-Intensive Industries," *Energy, Sustainability and Society*. 2018.
6. Zhang, Y., Sunarso, J., Liu, S. and Wang, R., "Current Status and Development of Membranes for CO_2/CH_4 Separation: A Review," *International Journal of Greenhouse Gas Control*. Elsevier January 1, 84-107(2013).
7. Khalilpour, R., Mumford, K., Zhai, H., Abbas, A., Stevens, G., Rubin, E. S., "Membrane-Based Carbon Capture from Flue Gas: A Review," *J. Clean. Prod.*, **103**, 286-300(2015).
8. Buonomenna, M. G., "Membrane Separation of CO_2 from Natural Gas," *Recent Patents Mater. Sci.*, 10(1), (2017).
9. Adewole, J. K., Ahmad, A. L., Ismail, S. and Leo, C. P., "Current Challenges in Membrane Separation of CO_2 from Natural Gas: A Review," *International Journal of Greenhouse Gas Control*. Elsevier September 1, 2013, 46-65.
10. Bazhenov, S. D., Bildyukevich, A. V. and Volkov, A. V., "Gas-Liquid Hollow Fiber Membrane Contactors for Different Applications," *Fibers*. Multidisciplinary Digital Publishing Institute October 10, 2018, 76.
11. Hafeez, S., Safdar, T., Pallari, E., Manos, G., Aristodemou, E., Zhang, Z., Al-Salem, S. M. and Constantinou, A., "CO_2 Capture Using Membrane Contactors: A Systematic Literature Review," *Frontiers of Chemical Science and Engineering*. 2021, 720-754.
12. Nogalska, A., Trojanowska, A. and Garcia-Valls, R., "Membrane Contactors for CO_2 Capture Processes - Critical Review," *Phys. Sci. Rev.*, **2**(7), 1-7(2019).
13. Siagian, U. W. R., Raksajati, A., Himma, N. F., Khoiruddin, K. and Wenten, I. G., "Membrane-Based Carbon Capture Technologies: Membrane Gas Separation vs. Membrane Contactor," *J. Nat. Gas Sci. Eng.*, **67**(April), 172-195(2019).
14. Sridhar, S., Smitha, B. and Aminabhavi, T. M., "Separation of Carbon Dioxide from Natural Gas Mixtures through Polymeric Membranes - A Review," *Separation and Purification Reviews*., 2007, 113-174.
15. Sainath, K., Modi, A. and Bellare, J., "CO_2/CH_4 Mixed Gas Separation Using Graphene Oxide Nanosheets Embedded Hollow Fiber Membranes: Evaluating Effect of Filler Concentration on Performance," *Chem. Eng. J. Adv.*, **5**, 100074(2021).
16. Vu, D. Q., Koros, W. J. and Miller, S. J., "High Pressure CO_2/CH_4 Separation Using Carbon Molecular Sieve Hollow Fiber Membranes," *Ind. Eng. Chem. Res.*, **41**(3), 367-380(2002).
17. Sridhar, S., Veerapur, R. S., Patil, M. B., Gudasi, K. B. and Aminabhavi, T. M., "Matrimid Polyimide Membranes for the Separation of Carbon Dioxide from Methane," *J. Appl. Polym. Sci.*, **106**(3), 1585-1594(2007).
18. Lee, S., Binns, M., Lee, J. H., Moon, J. H., Yeo, J. G. Yeo, Y. K., Lee, Y. M. M. and Kim, J. K., "Membrane Separation Process for CO_2 Capture from Mixed Gases Using TR and XTR Hollow Fiber Membranes: Process Modeling and Experiments," *J. Memb. Sci.*, **541**, 224-234(2017).
19. Falbo, F., Brunetti, A., Barbieri, G., Drioli, E. and Tasselli, F., "CO_2/CH_4 Separation by Means of Matrimid Hollow Fibre Membranes," *Appl. Petrochemical Res.*, **6**(4), 439-450(2016).
20. Liu, Y., Liu, Z., Kraftschik, B. E., Babu, V. P., Bhuwania, N., Chinn, D. and Koros, W. J., Natural Gas Sweetening Using TEGMC Polyimide Hollow Fiber Membranes," *J. Memb. Sci.*, **632**, 119361 (2021).
21. Liu, Y.; Liu, Z.; Morisato, A.; Bhuwania, N.; Chinn, D.; Koros, W. J. Natural Gas Sweetening Using a Cellulose Triacetate Hollow Fiber Membrane Illustrating Controlled Plasticization Benefits," *J. Memb. Sci.*, **601**, 117910(2020).
22. Lin, H., VanWagner, E., Raharjo, R., Freeman, B. D. and Roman, I., "High-Performance Polymer Membranes for Natural-Gas Sweetening," *Adv. Mater.*, **18**(1), 39-44(2006).
23. Ibrahim, M. H., El-Naas, M. H., Zhang, Z. and Bruggen, B., "Van der. CO_2 Capture Using Hollow Fiber Membranes: A Review of Membrane Wetting," *Energy and Fuels*, **32**(2), 963-978(2018).

24. Scholz, M., Wessling, M. and Balster, J., Chapter 5. Design of Membrane Modules for Gas Separations; 2011, 125-149.
25. Ahmad, F., Lau, K. K., Lock, S. S. M., Rafiq, S., Khan, A. U. and Lee, M., "Hollow Fiber Membrane Model for Gas Separation: Process Simulation, Experimental Validation and Module Characteristics Study," *J. Ind. Eng. Chem.*, **21**, 1246-1257(2015).
26. Qadir, S., Hussain, A. and Ahsan, M., "A Computational Fluid Dynamics Approach for the Modeling of Gas Separation in Membrane Modules," *Processes*, **7**(7), 420(2019).
27. Ahmad, F., Lau, K. K., Shariff, A. M. and Murshid, G., "Process Simulation and Optimal Design of Membrane Separation System for CO_2 Capture from Natural Gas," *Comput. Chem. Eng.*, **36**(1), 119-128(2012).
28. Chu, Y. and He, X., "Process Simulation and Cost Evaluation of Carbon Membranes for CO_2 Removal from High-Pressure Natural Gas. *Membranes (Basel).*, **8**(4), 118(2018).
29. Bandehali, S., Sanaeepur, H., Amooghin, A. E. and Moghadassi, A., "Modeling and Simulation for Membrane Gas Separation Processes," In *Modeling in Membranes and Membrane-Based Processes*; John Wiley & Sons, Ltd, 2020, 201-235.
30. Shamsabadi, A. A., Kargari, A., Farshadpour, F. and Laki, S., "Mathematical Modeling of CO_2/CH_4 Separation by Hollow Fiber Membrane Module Using Finite Difference Method," *J. Membr. Sep. Technol.*, **1**, 19-29(2012).
31. Adewole, J. K. and Ahmad, A. L., "Process Modeling and Optimization Studies of High Pressure Membrane Separation of CO_2 from Natural Gas," *Korean J. Chem. Eng.*, **33**(10), 2998-3010(2016).
32. Nakao, A., Macedo, A. P. F., Versiani, B. M., De, Q. F., Araújo, O. and De Medeiros, J. L., "Modeling of Flowcharts of Permeation Through Membranes for Removal of CO_2 of Natural Gas," *Comput. Aided Chem. Eng.*, **27**(C), 1875-1880(2009).
33. Hosseini, S. S., Dehkordi, J. A. and Kundu, P. K., Gas Permeation and Separation in Asymmetric Hollow Fiber Membrane Permeators: Mathematical Modeling, Sensitivity Analysis and Optimisation," *Korean J. Chem. Eng.*, **33**(11), 3085-3101(2016).
34. Lock, S. S. M., Lau, K. K., Ahmad, F. and Shariff, A. M., "Modeling, Simulation and Economic Analysis of CO_2 Capture from Natural Gas Using Cocurrent, Countercurrent and Radial Crossflow Hollow Fiber Membrane," *Int. J. Greenh. Gas Control*, **36**, 114-134(2015).
35. Ahsan, M. and Hussain, A., "Mathematical Modelling of Membrane Gas Separation Using the Finite Difference Method," *Pacific Sci. Rev. A Nat. Sci. Eng.*, 18(1), 47-52(2016).
36. Hoorfar, M., Alcheikhhamdon, Y. and Chen, B., "A Novel Tool for the Modeling, Simulation and Costing of Membrane Based Gas Separation Processes Using Aspen HYSYS: Optimisation of the CO_2/CH_4 Separation Process," *Comput. Chem. Eng.*, **117**, 11-24(2018).
37. Gilassi, S., Taghavi, S. M., Rodrigue, D. and Kaliaguine, S., "Simulation of Gas Separation Using Partial Element Stage Cut Modeling of Hollow Fiber Membrane Modules," *AIChE J.*, **64**(5), 1766-1777(2018).
38. Feng, X., Ivory, J. and Rajan, V. S. V., "Air Separation by Integrally Asymmetric Hollow-Fiber Membranes," *AIChE J.*, **45**(10), 2142-2152(1999).

Authors

Boram Gu: Assistant professor, School of Chemical Engineering, Chonnam National University, 77 Yongbong-ro, Buk-gu, Gwangju, 61186, Korea; boram.gu@jnu.ac.kr